Cerna, Fernando V.; Pourakbari-Kasmaei, Mahdi; Contreras, Javier; Gallego, Luis A.

Optimal Selection of Navigation Modes of HEVs considering CO_2 Emissions Reduction

Published in:
IEEE Transactions on Vehicular Technology

DOI:
10.1109/TVT.2019.2894383

Published: 01/03/2019

Document Version
Peer-reviewed accepted author manuscript, also known as Final accepted manuscript or Post-print

Please cite the original version:
Cerna, F. V., Pourakbari-Kasmaei, M., Contreras, J., & Gallego, L. A. (2019). Optimal Selection of Navigation Modes of HEVs considering CO_2 Emissions Reduction. *IEEE Transactions on Vehicular Technology*, *68*(3), 2196-2206. Article 8620548. https://doi.org/10.1109/TVT.2019.2894383

Optimal Selection of Navigation Modes of HEVs considering CO_2 Emissions Reduction

Fernando V. Cerna, Mahdi Pourakbari-Kasmaei, *Member, IEEE*, Javier Contreras, *Fellow, IEEE*, and Luis A. Gallego, *Member, IEEE*

***Abstract*—In this paper, a mixed-integer linear programming (MILP) model is proposed to optimize hybrid electric vehicle (HEV) navigation modes on the city map, namely the problem of the optimal selection of navigation modes (OSNMs). The OSNMs problem of the HEV as part of the operating strategy is obtained considering a constraint set related to CO_2 emissions reduction, efficient battery charging, and the optimal scheduling of deliveries. Uncertainties in the HEV navigation on urban roads are modeled using probability values assigned to an established set of traffic density values according to the levels of service (LOS). The model is implemented in AMPL and solved using the commercial solver CPLEX. The case study considers real data related to the Prius Prime technology and shows the effectiveness of automating the HEV navigation modes considering CO_2 emissions reduction levels during an operating strategy.**

***Index Terms*—Efficient battery charging, optimal selection navigation modes, optimal scheduling of deliveries, operating strategy.**

NOMENCLATURE

A. Sets

Ω_i	Set of intersections *i*.
Ω_{ur}	Set of urban roads *ki*.
Ω_D	Set of density values *u*.

B. Parameters

au	Autonomy (km).
d_{ki}	Length of urban road *ki* (km).
D_{ki}	Traffic density in each urban road *ki* (veh/km).
D_u	Value of the traffic density of element *u* (veh/km).
D_J	Saturation density (veh/km).
D_0	Optimal density related to F_{max} (veh/km).
E^{CO_2}	CO_2 emissions (gCO_2/km).
F_{max}	Maximum traffic flow (veh/h).
F_{max}^{mr}	Maximum traffic flow in main roads (veh/h).
F_{max}^{sr}	Maximum traffic flow in secondary roads (veh/h).
K^E	Battery energy capacity (kWh).
K^C	Tank fuel capacity (L).
M	Big value used in the linearization process.
$MR_{r,d}$	Matrix of possible routes.
N^d	Number of deliveries.
N^p	Total number of periods.
NR	Number of possible routes.
P^{ch}	Charging rate of the HEV (kW).
P_u^{mr}/P_u^{sr}	Probability values related to traffic density *u* in main/secondary roads, respectively.
P_u^{amr}/P_u^{asr}	Accumulated probability related to P_u^{mr}/P_u^{sr}.
r_i^s	Location of the charging station (0/1: intersection *i* without/with charging station).
SOC^o	Initial state of charge of the battery of HEV (kWh).
$t_{d,i}^n$	Type of intersection *i* in delivery *d* (-1: starting; 0: intermediate; 1: arrival).
t_{ki}^{ur}	Type of urban road *ki* (1: main; 0: secondary).
$\overline{v}_{ki}$	Maximum average speed in urban road *ki* (km/h).
v_f	Free flow speed (km/h).
v_0	Optimal speed related to F_{max} (km/h).
v_0^{mr}/v_0^{sr}	Optimal speed related to $F_{max}^{mr}/F_{max}^{sr}$ (km/h).
δ^{km}, δ^{hx}	Maintenance costs (\$/km) and extra hours cost (\$/h).
Δt	Duration of each period (h).
δ^C	Fuel expense (km/L).
ρ^C	Levels of CO_2 emissions reduction.
τ^{max}	Maximum limit of total operating time (h).
δ^{PE}	Percentage of energy that defines the state of charge of the HEV at the arrival intersection (warehouse).
δ^D	Energy spent during navigation of the HEV (kWh/km).
$\overline{\tau}^{ch}/\underline{\tau}^{ch}$	Upper/lower limits of the charging time (h).
η^{cE}/η^{dE}	Charging/discharging efficiencies.

C. Variables

$\omega_{d,ki}$	Binary variable that indicates the navigation of the HEV in urban road *ki* for delivery *d*.
$n_{d,ki}$	Integer variable indicating the number of periods during navigation of the HEV in urban road *ki* for delivery *d*.
$v_{d,ki}$	Average speed value in the navigation of the HEV in urban road *ki* for delivery *d* (km/h).
$d_{d,ki}^{SM}, d_{d,ki}^{DM}$	Length of urban road *ki* for delivery *d* traveled in a charge-sustaining, and charge-depleting mode (km).
$\Delta\tau$	Extra hours related to the HEV (h).
$SOC_{d,i}$	State of charge of the battery of the HEV at intersection *i* for delivery *d* (kWh).
$SOC_{d,i}^a$	State of charge of the battery of HEV at the moment of arrival at intersection *i* for delivery *d* (kWh).
$\varepsilon_{d,i}$	Total energy for the charging of the HEV at intersection *i* for delivery *d* (kWh).

This work was supported by the Brazilian Institutions CAPES, No. 1699327/2017, and FAPESP, Nos. 2014/22828-3 and 2016/14319-7.

F. V. Cerna, and Luis A. Gallego are with the Department of Electrical Engineering, State University of Londrina (UEL), Londrina 86057-970, PR, Brazil (e-mail: fvcerna83@gmail.com; gallegopareja@gmail.com).

Mahdi Pourakbari-Kasmaei is with the Department of Electrical Engineering and Automation, Aalto University, 02150 Espoo, Finland (e-mail: Mahdi.Pourakbari@aalto.fi).

Javier Contreras is with E.T.S. de Ingenieros Industriales, University of Castilla–La Mancha, 13071 Ciudad Real, Spain (e-mail: Javier.Contreras@uclm.es).

$\tau_{d,i}^{ch}$ Charging time of the HEV at intersection i for delivery d (h).

$y_{d,i}$ Binary variable that indicates the charging status of the HEV at intersection i for delivery d.

$\alpha_{d,ki,t}$ Binary variable used in the discretization of $n_{d,ki}$.

$\Delta\alpha_{d,ki,t}$ Continuous variable that represents the product of $v_{d,ki}$ and $\alpha_{d,ki,t}$ in the linearization process.

$\Delta\omega_{d,ki}^{DM}$ Continuous variable that represents the product of $\omega_{d,ki}$ and $d_{d,ki}^{DM}$ in the linearization process.

$\Delta'_{d,ki}$ Continuous variable that represents the product of $\omega_{d,ki}$ and $SOC_{d,k}$ in the linearization process.

$\Delta\tau_{d,i}^{ch}$ Continuous variable that represents the product of $y_{d,i}$ and $\tau_{d,i}^{ch}$ in the linearization process.

I. Introduction

The hybrid electric vehicle (HEV) represents an efficient and viable means of transportation that may help to reduce CO_2 emissions during navigation, ensuring the optimal energy management in future smart cities [1]. Basically, an HEV has two navigation modes, namely, charge-sustaining mode (SM) in which the HEV consumes fuel, and charge-depleting mode (DM) where the HEV uses its battery, which determine the energy state of the battery and the locomotion system [2]. In the service sector, several applications for HEVs exist, mainly for emergency and delivery services [3], [4]. In the performance of HEVs during operation, traffic information (flow and density of traffic) along a given period and the uncertainties for each type of service should be considered [5]. Thus, to take full advantage of the potential of each HEV, the development of an operational strategy is essential. An appropriate selection of the navigation mode (SM or DM), efficient battery recharge, and optimal scheduling of deliveries should be considered as part of this strategy [4], [6]. Therefore, this paper aims at developing an intelligent tool to ensure the optimal selection of navigation modes (OSNMs) of HEVs considering time constraints, speed limits on urban roads, and energy requirements of the HEVs for different levels of CO_2 emissions reduction.

In literature, most of the studies only address economic issues, and works related to the optimal performance of HEVs that specifically consider the navigation modes on urban roads during operation (deliveries to the specified points) on a city map taking into account environmental issues are scarce. In [1], a predictive control model of the torque and speed of an HEV to manage the energy consumption during the trip was developed. In [2], another approach aimed at minimizing the fuel consumption based on the selection of appropriate driving modes was presented. In this approach, the trip information integrated into path planning, and charging stations was used to analyze the Chevrolet Volt performance, while ignoring the impact of extra hours, as well as the distances traveled in each driving mode during the operation. An engine management strategy to control the pollutant effect of CO_2 emissions on pedestrians along a specified route was developed in [3]. This strategy was used for testing the Toyota Prius performance in four prespecified routes on the city map; while in the city area, there were no charging points along the routes, all the routes presented the same starting points, and the arrival points did not have any connection. In [4], an MILP model was proposed to minimize the extra hours and maintenance costs while making a set of prespecified deliveries on a city map. This model was used to evaluate the performance of a fleet of EVs considering the fast and ultra-fast charging rates during operation. A multi-objective model to find the optimal charging and navigation strategy considering the traffic congestion, power network operation, and the number of charging stations at each node was developed in [6]. In [7], a proper framework was proposed for plug-in HEVs to optimally allocate the limited charging stations among metropolitan areas via adequate interactions among public charging availability, electricity prices, and destination and route choices. Maximizing social welfare was the primary goal of this work, where an active-set algorithm along with a nonlinear commercial solver was used to solve the model. A solid framework was proposed in [8], wherein the transportation and electric power networks were considered simultaneously. In this paper, a convex model was developed to handle the joint consideration of rational route choices, fast charging stations, and marginal electricity pricing. The path planning problem for the HEVs considering two aspects of energy usage and battery was proposed in [9], [10]. Similarly, another model aimed at evaluating the performance of HEVs concerning the internal combustion engine vehicle (ICE) was developed in [11]. Furthermore, in some works, the charging of HEVs at specific points located along the main path was considered while taking into account traffic flow information for the assignment of HEVs to the charging points. Charging strategies were developed in [12]–[14], aimed at minimizing the charging costs of EVs, and establishing the policies to determine the optimal scheduling considering historical trip data. Also, some works aimed at minimizing emissions and fuel costs, via dynamic programming (DP), sustainable transportation models, and predictive strategies were proposed in [15]–[18]. In [19], [20] two algorithms for optimal control and fuel cost minimization considering drivability of the HEVs were developed. In [21], an online energy management model that used the speed profile prediction and multiple trips of varying length with onboard trip information aimed at obtaining an estimated fuel savings was proposed. Similarly, a stochastic model of [21] for HEVs with specified routes was solved in [22]. In this work, a time-varying scaling method to generate fixed-route driving data was used. A pseudospectral algorithm was developed in [23] to optimize the HEV power management. The charging rate profile in the powertrain of the HEVs, as well as the maximum demand, power grid limits, and driver satisfaction were considered in [24]. A DP algorithm was used in [25] to minimize the equivalent fuel consumption considering the optimal shift scheduling and energy management mode of HEVs during a driving cycle.

The navigation system information (GPS/GIS) allows us to determine a control strategy between engines and batteries to find the optimal power flow in powertrain operation for a full cycle. Moreover, traditional optimization methods are not robust enough to face dynamic changes, and usually, a complete restart must be provided to obtain a feasible solution (e.g., DP). In contrast, evolutionary algorithms are used in such changing

TABLE I
COMPARISON OF PREVIOUS MODELS AND THE PROPOSED MODEL

Features	Previous Model [4]	Proposed Model
Navigation modes	Fully electric	SM and DM
Sequence of deliveries	An established sequence exists	Considers all possible sequences
Charging rate	Variable	Constant
CO_2 emissions	No	Yes (Reduction levels)
Uncertainties during navigation	Presence of traffic signals, schools, and public works	Traffic density variation considering LOS

circumstances. However, none of them can guarantee finding the optimal global solution [26]. On the whole, to address the existing drawbacks and shortcomings in the navigation sector, a smart management system may play a vital role.

This paper proposes an MILP model to find the OSNMs (SM and DM) of an HEV during its operation on the city map by minimizing the maintenance and extra hour costs. In the proposed model, reducing CO_2 emissions, efficient battery charging, and optimal scheduling of deliveries constitute the operating strategy to ensure the OSNMs of the HEV. Thus, constraints related to the set of possible routes for deliveries, battery capacity, speed variation, charging and discharging efficiencies, as well as the levels of CO_2 emissions reduction, are considered. An iterative process is used to evaluate the OSNMs of the HEV for all possible operation strategies. Uncertainties in the HEV navigation on the city map, which are the result of traffic density variation, are modeled using probability values related to the levels of service (LOS). The city map is modeled as a graph with 71 nodes (intersections) and 131 edges (main and secondary roads). The case study that considers data of the real Prius Prime technology shows promising results on how to automate the selection of the navigation modes of this hybrid technology. The proposed model is implemented in the AMPL language and the commercial solver CPLEX is used to find the optimal solution.

This paper extends the proposed model in [4] that is solely related to the battery electric vehicle (BEV) performance during navigation on the city map. Thus, driving of EVs in full electric mode represents only a part of the EVs navigation modes. Therefore, a more complete model should consider the main navigation modes such as SM and DM.

In this way, the proposed model considers these navigation modes of the HEVs, as well as their optimal selection during the trip along urban roads, taking into account the levels of CO_2 emissions reduction, among other features shown in Table I. Therefore, the main contributions of this paper are threefold:

- Proposing an MILP model for the OSNMs of an HEV during operation considering CO_2 emissions reduction levels with an efficient computational behavior using conventional MILP solvers.
- The optimization model is flexible and guarantees the OSNMs of the HEVs considering all possible operation strategies so that they can be charged at charging points on the city map.
- From a sustainable perspective, the application of an intelligent tool contributes to fuel consumption economy as well as to the minimization of pollutants.

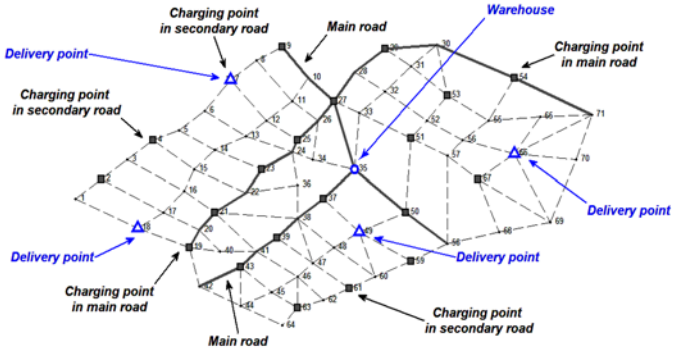

Fig. 1. Charging and delivery points on the city map.

The rest of this paper is organized as follows. Section II presents the hypotheses and uncertainties in the navigation. The proposed MINLP model and the linearization process to obtain the MILP model are presented in section III. Section IV contains the case study and results. Section V presents the conclusions.

II. MATHEMATICAL MODELING

This section contains the hypotheses related to the charging infrastructure, delivery points, and the uncertainties represented by the speed variation as a function of traffic density.

A. Hypotheses

To obtain more practical results, the following hypotheses are used to solve the problem [5], [27]–[32].

1. Charging infrastructure exists on the city map. The charging stations have been optimally placed in the electric power distribution network.
2. Locations of the charging and delivery points on the city map are known.
3. A single point, namely warehouse, represents the departure and arrival points of the HEV.
4. Speed variations depend on the uncertainties in traffic density.
5. Traffic density values for each type of urban road are calculated only once and represent part of the input data to the MILP model.

B. Modeling of Charging Infrastructure and Delivery Points

In this section, the location of the charging and delivery points is modeled as in [4]. Urban road *ki* is differentiated by t_{ki}^{ur}, which characterizes a main or a secondary urban road on the city map [33]. Fig. 1 shows the number of charging points (in gray squares) located ($r_i^s = 1$) along the main road (gray line) with a minimum separation of eight kilometers. On secondary roads (dashed lines), charging points are located at intersections i ($r_i^s = 1$) near the main road. Warehouse and delivery points are represented by circles and triangles in blue, respectively. Each delivery d located at intersection i on the city map is characterized by $t_{d,i}^n$, which can adopt values of -1 or 1. Thus, the same intersection i may present $t_{d,i}^n = 1$ (arrival intersection), and $t_{d+1,i}^n = -1$ (departure intersection) values for deliveries d, and d+1, respectively. The locations of charging and delivery points, and the warehouse are available in [34].

C. Uncertainties Simulation

Traffic density variation represents the uncertainties in the navigation of the HEVs. This variation in the number of

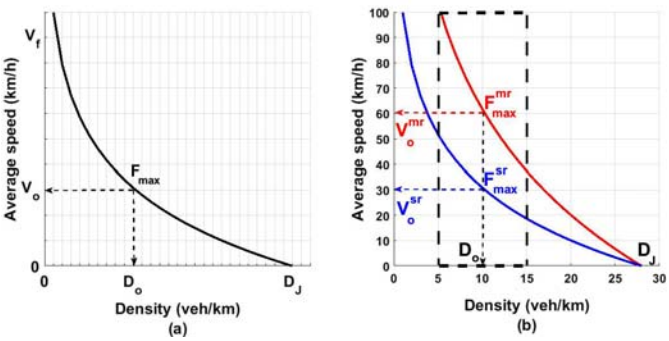

Fig. 2. Speed-density characteristic curve.

vehicles per kilometer of road ki determines the speed of navigation of the HEVs on this [4], [5].

The shape of the speed-density curve, as well as its main parameters, are shown in Fig. 2 (a). Similarly, in Fig. 2 (b) the curves considered for representing the speed variation on main and secondary urban roads are shown. These curves are defined by (1)-(3) [35].

$$\overline{v}_{ki} = v_0 Ln(\frac{D_J}{D_{ki}}) \quad (1)$$

$$F_{max} = \frac{v_0 D_J}{e} \quad (2)$$

$$D_0 = \frac{D_J}{e} \quad (3)$$

Due to (1), curve $\overline{v}_{ki}$ is inversely proportional to D_{ki}, and point (D_o, v_o) determines the maximum capacity of traffic flow, F_{max}, related to urban road ki, as seen in Fig. 2(a). In Fig. 2 (b), the speed-density curves, related to the secondary ($t_{ki}^{ur} = 0$) and main ($t_{ki}^{ur} = 1$) roads are depicted in blue and red, respectively.

To simulate the uncertainties during the operation of the HEV, the density variation interval (enclosed in dashed lines) shown in Fig. 2 (b) is considered. In this interval, traffic densities are differentiated by letters A-C named LOS [5], [35], where A indicates a low traffic density, B stands for speed restricted by traffic, and C represents speed limited by a high traffic density. Because the traffic density is stochastic, uncertainty should be taken into account. In this work, stochasticity is handled externally, using random numbers. Thus, traffic density values, D_u, are assigned to the main and secondary urban roads through the probability values P_u^{mr} and P_u^{sr} for the main and secondary roads, respectively [34].

To represent the influence of the uncertainties related to the traffic density during operation of the HEV, the proposed simulation algorithm is portrayed in Fig. 3. Values v_o^{mr} and v_o^{sr} are assumed to be 60 and 30, respectively. These values correspond to the arterial and local roads applied in different states in the United States and Brazil that have been derived from practical reports [27], [36]. Thus, the proposed algorithm starts with a set of established values, P_u^{amr}, P_u^{asr}, D_u, D_J, v_o^{mr}, v_o^{sr}, and the values D_{ki} and $\overline{v}_{ki}$ are initialized to zero. Then, an iterative process is carried out for all urban roads, ki. Thereafter, random values between 0 and 100 are assigned to n^{al}. Each random value generated is evaluated under the condition $n^{al} \neq 0$, ensuring random values greater than zero. Next, the values of t_{ki}^{ur} for each urban road are compared under the condition $t_{ki}^{ur} = 1$, if the condition is Yes, then an iterative process that calculates $\overline{v}_{ki}$ for the main urban roads is done,

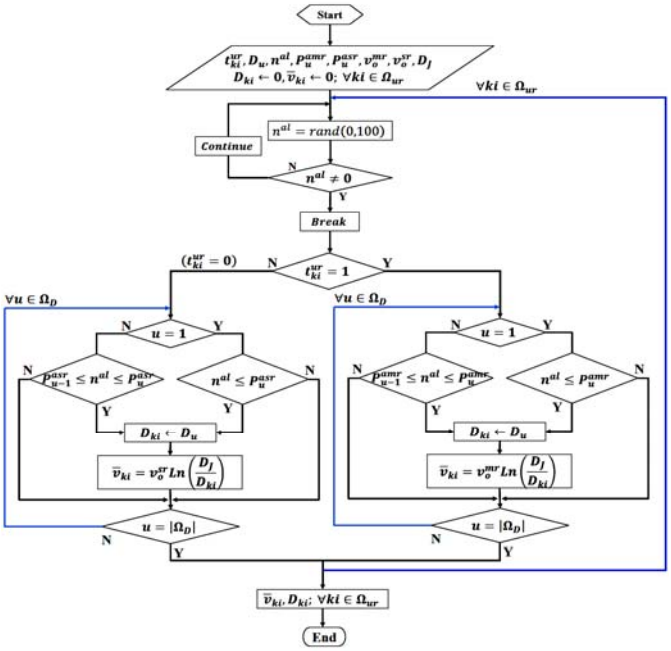

Fig. 3. Flowchart of the simulation algorithm.

otherwise, the process is done for the secondary roads ($t_{ki}^{ur} = 0$). Note that for both values of t_{ki}^{ur}, the iterative process (for all elements u of Ω_D) is similar, it is only necessary to change the values P_u^{amr} and v_o^{mr} of the main urban roads to P_u^{asr} and v_o^{sr} of the secondary urban roads. Now, the iterative process to assign traffic density values only on main urban roads is explained. Condition $u = 1$ indicates that, for the first value of u, the number n^{al} is evaluated under condition $n^{al} \leq P_u^{amr}$, if this condition is satisfied (Yes), then D_u is assigned to D_{ki} and $\overline{v}_{ki}$ is calculated, otherwise, a new iteration u ($u > 1$) is done. For the case $u > 1$, n^{al} is evaluated for condition $P_{u-1}^{amr} \leq n^{al} \leq P_u^{amr}$, if this condition is Yes, then D_{ki} is assigned to its respective D_u and $\overline{v}_{ki}$ is computed, otherwise, the iterations for u continue until the stopping criterion $u = \Omega_D$ is satisfied. Once the stopping criterion is reached the process continues to the next iteration related to urban road ki. Finally, as a result of the iterative process the values of D_{ki} and $\overline{v}_{ki}$ are obtained for each urban road, ki, and these values are used as the input data in constraint (10) of the MILP model.

III. Proposed Model

The proposed model is formulated initially as an MINLP problem, (4)–(25).

$$min: \ \delta^{hx}\Delta\tau + \ \delta^{km}\sum_{d=1}^{N^d}\sum_{\forall ki\in\Omega_{ur}} d_{ki}\omega_{d,ki} \quad (4)$$

The total costs related to extra hours and maintenance costs for the HEV are minimized in (4). Thus, the objective function in (4) has two components. The first one is related to the optimization of the delay times. The extra hours in this term, $\Delta\tau$, are the result of speed variation or waiting times due to the traffic density, or the delay time during the HEV battery charging process. A detailed explanation related to the calculation of extra hours is provided in (11). Because traffic density is a stochastic phenomenon, this component has a greater influence on the minimization of the HEV charging times. Therefore, this first component allows for an implicit

minimization of the HEV's battery charging costs considering the case in which the extra hours, $\Delta\tau$, are also influenced by the time delay generated as a part of the total time of recharges made by the HEV, the second term on the left side of the constraint. Thus, an implicit way to minimize the charging costs during the HEV operation is to reduce the number of charging by visiting the least possible number of charging points. The second component ensures that the urban roads of the possible routes are the shortest. In this term, variables $y_{d,i}$ and $\tau_{d,i}^{ch}$, that respectively represent the recharge ($y_{d,i}=1$) or non-recharge ($y_{d,i}=0$) state, as well as the charging time of the HEV battery at intersection i ($r_i^s=1$), ensure a shorter recharge time at each charging point to be visited ($r_i^s=1$ and $y_{d,i}=1$). In this way, the lifetime of the HEV is implicitly optimized in the proposed model. The constraints of this problem are as follows.

$$\sum_{ki\in\Omega_{ur}}\omega_{d,ki}-\sum_{ij\in\Omega_{ur}}\omega_{d,ij}=-1;\ \forall d\in 1..N^d,\ \forall i\in\Omega_i/\ t_{d,i}^n=-1 \quad (5)$$

$$\sum_{ki\in\Omega_{ur}}\omega_{d,ki}-\sum_{ij\in\Omega_{ur}}\omega_{d,ij}=0;\ \forall d\in 1..N^d,\ \forall i\in\Omega_i/\ t_{d,i}^n=0 \quad (6)$$

$$\sum_{ki\in\Omega_{ur}}\omega_{d,ki}-\sum_{ij\in\Omega_{ur}}\omega_{d,ij}=1;\ \forall d\in 1..N^d,\ \forall i\in\Omega_i/\ t_{d,i}^n=1 \quad (7)$$

Constraints (5)-(11) are related to determining the optimal scheduling of deliveries d to be done by the HEV. Constraint (5) is used to obtain the shortest urban road d_{ij} to be traveled, from intersection i ($t_{d,i}^n=-1$) to all possible intersections j. Constraint (6) is related to the navigation of the HEV on urban roads formed with intermediate intersections, where the navigation from intersections k to i and i to j constitutes a minimum route, d_{ki}, and d_{ij}. In this case, an intermediate intersection i ($t_{d,i}^n=0$) represents the arrival intersection for the HEV coming from all possible intersections k, and at the same time, it represents the departure intersection for the HEV going to all possible intersections j. In (7), urban road ki is selected such that the length that must be traveled, starting from all possible intermediate intersections k ($t_{d,k}^n=0$) to the arrival intersection i ($t_{d,i}^n=1$), is the shortest, d_{ki}. Constraints (8)-(11) refer to the number of periods and speed values on each urban road ki during operation of the HEV. Equation (8) shows that the length of the selected urban road ki, $d_{d,ki}\omega_{d,ki}$, is proportional to the speed, $v_{d,ki}$, and the total time, $n_{d,ki}\Delta t$, in which the urban road ki will be traversed by the HEV. Note that once the urban road ki ($\omega_{d,ki}=1$) is selected, its length, $d_{d,ki}$, is known. Thus, the navigation time value ($n_{d,ki}\Delta t$) will depend solely on the value of the speed, $v_{d,ki}$. In (9), the non-negativity of $n_{d,ki}$, is guaranteed. Constraint (10) guarantees the speed limits, $\overline{v_{ki}}$, obtained through the process depicted in Fig. 3. In (11), the total operating time is composed of $n_{d,ki}\Delta t$ and $y_{d,i}\tau_{d,i}^{ch}$, which are the navigation times due to the influence of uncertainties on traffic density, and the charging times, which depend on $P_{d,i}^{ch}$ and $SOC_{d,i}$ of HEV, respectively. The sum of these times should not exceed the maximum limit, τ^{max}. In case this limit is exceeded, there will be $\Delta\tau$ extra hours during the HEV operation and, since there is a corresponding penalty to this term in the objective function, (4), the model tries to keep it as low as possible.

$$d_{ki}\omega_{d,ki}=v_{d,ki}n_{d,ki}\Delta t;\ \forall d\in 1..N^d,\forall ki\in\Omega_{ur} \quad (8)$$

$$0\le n_{d,ki};\ \forall d\in 1..N^d,\forall ki\in\Omega_{ur} \quad (9)$$

$$0\le v_{d,ki}\le\overline{v}_{ki};\ \forall d\in 1..N^d,\forall ki\in\Omega_{ur} \quad (10)$$

$$\sum_{d=1}^{N^d}\sum_{\forall ki\in\Omega_{ur}}n_{d,ki}\Delta t+\sum_{d=1}^{N^d}\sum_{\forall i\in\Omega_i/t_{d,i}^n\ge 0}y_{d,i}\tau_{d,i}^{ch}\le\tau^{max}+\Delta\tau \quad (11)$$

The constraints related to the efficient battery charging of the HEVs are determined by (12)-(21). In (12), the initial state of charge, SOC^0, at intersection i ($t_{d,i}^n=-1$) for the first delivery d, is considered. $SOC_{d,i}$ for delivery d at intersection i ($t_{d,i}^n\ge 0$) is calculated in (13). In this calculation, the available energy, $SOC_{d,i}^a$, and the energy to be recharged by the HEV at the charging points located at intersection i ($r_i^s=1$), $\varepsilon_{d,i}$, is considered. The state of charge, $SOC_{d-1,i}$, for the battery of the HEV for delivery $d-1$ at intersection i ($t_{d-1,i}^n=1$) is equal to its SOC for delivery d at intersection i ($t_{d,i}^n=-1$), (14). In (15), the final state of charge, $SOC_{d,i}$ at intersection i ($t_{d,i}^n=1$), after returning ($d=N^d$) to the warehouse, is established. In (16), the limits of $SOC_{d,i}$ are guaranteed.

$$SOC_{d,i}=SOC^o;\ \forall d\in 1..N^d,\forall i\in\Omega_i/\ d=1\ \wedge\ t_{d,i}^n=-1 \quad (12)$$

$$SOC_{d,i}=SOC_{d,i}^a+\varepsilon_{d,i};\ \forall d\in 1..N^d,\forall i\in\Omega_i/\ t_{d,i}^n\ge 0 \quad (13)$$

$$SOC_{d,i}=SOC_{d-1,i};\ \forall d\in 1..N^d,\forall i\in\Omega_i/\ d>1\ \wedge t_{d,i}^n=-1\ \wedge\ t_{d-1,i}^n=1 \quad (14)$$

$$SOC_{d,i}=\delta^{PE}K^E;\ \forall d\in 1..N^d,\forall i\in\Omega_i/\ d=N^d\ \wedge\ t_{d,i}^n=1 \quad (15)$$

$$0\le SOC_{d,i}\le K^E;\ \forall d\in 1..N^d,\forall i\in\Omega_i \quad (16)$$

In (17), the available energy in the battery, $SOC_{d,i}^a$, is calculated as the difference between $SOC_{d,k}$ at intersection k and $\eta^{dE}\delta^D d_{d,ki}^{DM}$, which is the energy used during travel in DM on urban road ki ($\omega_{d,ki}=1$). The non-negativity of $SOC_{d,i}^a$ is guaranteed in (18) at intersection i.

$$SOC_{d,i}^a=\sum_{ki\in\Omega_{ur}}\omega_{d,ki}\left(SOC_{d,k}-\eta^{dE}\delta^D d_{d,ki}^{DM}\right);\ \forall d\in 1..N^d,\forall i\in\Omega_i \quad (17)$$

$$0\le SOC_{d,i}^a;\ \forall d\in 1..N^d,\forall i\in\Omega_i \quad (18)$$

Constraint (19) guarantees that no charge is necessary at the starting intersection i ($t_{d,i}^n=-1$) for the first delivery d and for subsequent deliveries at intersection i ($t_{d,i}^n\ge 0$) without charging points ($r_i^s=0$), respectively. The recharge energy, $\varepsilon_{d,i}$, is calculated in (20) where the charging depends on variables $y_{d,i}$, and $\tau_{d,i}^{ch}$ at each intersection i in the presence of a charging point ($r_i^s=1$). Constraint (21) guarantees that $\tau_{d,i}^{ch}$ remains between the lower and upper limits, respectively.

$$\varepsilon_{d,i}=0;\ \forall d\in 1..N^d,\forall i\in\Omega_i/\left(d=1\ \wedge\ t_{d,i}^n=-1\right)\vee\left(t_{d,i}^n\ge 0\ \wedge\ r_i^s=0\right) \quad (19)$$

$$\varepsilon_{d,i}=\eta^{cE}P^{ch}y_{d,i}\tau_{d,i}^{ch};\ \forall d\in 1..N^d,\forall i\in\Omega_i/\ t_{d,i}^n\ge 0\wedge r_i^s=1 \quad (20)$$

$$\underline{\tau}^{ch}\le\tau_{d,i}^{ch}\le\overline{\tau}^{ch};\ \forall d\in 1..N^d,\forall i\in\Omega_i \quad (21)$$

Constraints related to CO_2 emissions reduction levels are established in (22)-(25). In (22), the sum of the lengths of urban road *ki* for delivery *d* that is traveled in DM ($d_{d,ki}^{DM}$) and SM ($d_{d,ki}^{SM}$) must be equal to the length of the urban road to be traveled (d_{ki}) for delivery *d* and each urban road *ki*. In constraints (23) and (24), the non-negativity of these lengths is guaranteed.

$$d_{ki}\omega_{d,ki} = d_{d,ki}^{DM} + d_{d,ki}^{SM}; \forall d \in 1..N^d, \forall ki \in \Omega_{ur} \quad (22)$$

$$0 \le d_{d,ki}^{DM}; \forall d \in 1..N^d, \forall ki \in \Omega_{ur} \quad (23)$$

$$0 \le d_{d,ki}^{SM}; \forall d \in 1..N^d, \forall ki \in \Omega_{ur} \quad (24)$$

$$0 \le E^{CO_2} \sum_{d=1}^{N^d} \sum_{ki \in \Omega_{ur}} \left((1-\rho^C)\omega_{d,ki} d_{ki} - d_{d,ki}^{SM}\right) \quad (25)$$

The relationship between the kilometers traveled in SM, $d_{d,ki}^{SM}$, and the total number of kilometers, d_{ki}, for each urban road *ki* to be traveled in delivery *d*, are established in (25). This relationship is determined by the CO_2 emissions reduction level, ρ^C. Thus, an increase in the ρ^C values represents that CO_2 emissions in SM must be less than $(1-\rho^C)$ times the total CO_2 emissions during the operation of the HEV. Constraint (25) allows us to determine the OSNMs of the HEV for each level, ρ^C. Thus, if $d_{d,ki}^{SM}$ decreases, then, a lower fuel consumption (consequently, less emission of pollutant gases) and a more frequent use of the HEV battery (increase in the $d_{d,ki}^{DM}$ values), are obtained during navigation of the HEV for each operating strategy.

A. Linearization

In the proposed model, the Big-M method is used to linearize non-linear constraints (8), (11), (17) and (20), [26], [37]. To linearize constraint (8), $n_{d,ki}$ is discretized with N^P binary variables $\alpha_{d,ki,t}$ in (26.b) and used in (26.a). Also, the linearization technique in [4] is used in (26.c)-(26.d).

$$d_{ki}\omega_{d,ki} = \Delta t \sum_{t=1}^{N^P} \Delta\alpha_{d,ki,t}\,;\ \forall d \in 1..N^d, \forall ki \in \Omega_{ur} \quad (26.a)$$

$$n_{d,ki} = \sum_{t=1}^{N^P} \Delta\alpha_{d,ki,t}\,;\ \forall d \in 1..N^d, \forall ki \in \Omega_{ur} \quad (26.b)$$

$$0 \le -\Delta\alpha_{d,ki,t} + v_{d,ki} \le M\left(1-\alpha_{d,ki,t}\right); \forall d \in 1..N^d, \forall ki \in \Omega_{ur}, \forall t \in 1 \dots N^P \quad (26.c)$$

$$0 \le \Delta\alpha_{d,ki,t} \le M\alpha_{d,ki,t}; \forall d \in 1..N^d, \forall ki \in \Omega_{ur}, \forall t \in 1 \dots N^P \quad (26.d)$$

Constraint (17) is replaced with (27.a) and the set of linear constraints (27.b)-(27.e) is considered.

$$SOC_{d,i}^a = \sum_{ki \in \Omega_{ur}} (\Delta'_{d,ki} - \delta^D \Delta\omega_{d,ki}^{DM})\,;\ \forall d \in 1..N^d, \forall i \in \Omega_i \quad (27.a)$$

$$0 \le -\Delta'_{d,ki} + SOC_{d,k} \le M * \left(1-\omega_{d,ki}\right); \forall d \in 1..N^d, \forall ki \in \Omega_{ur} \quad (27.b)$$

$$0 \le \Delta'_{d,ki} \le M\omega_{d,ki}; \quad \forall d \in 1..N^d, \forall ki \in \Omega_{ur} \quad (27.c)$$

$$0 \le -\Delta\omega_{d,ki}^{DM} + d_{d,ki}^{DM} \le M\left(1-\omega_{d,ki}\right); \quad \forall d \in 1..N^d, \forall ki \in \Omega_{ur} \quad (27.d)$$

$$0 \le \Delta\omega_{d,ki}^{DM} \le M\omega_{d,ki}; \quad \forall d \in 1..N^d, \forall ki \in \Omega_{ur} \quad (27.e)$$

In the linearization of (20), constraints (28.a)-(28.c) are used.

$$\varepsilon_{d,i} = \eta^{cE} P^{ch} \Delta\tau_{d,i}^{ch}; \forall d \in 1..N^d, \forall i \in \Omega_i / t_{d,i}^n \ge 0 \wedge r_i^s = 1 \quad (28.a)$$

$$0 \le -\Delta\tau_{d,i}^{ch} + \tau_{d,i}^{ch} \le M\left(1-y_{d,i}\right); \forall d \in 1 \dots N^d, \forall i \in \Omega_i \quad (28.b)$$

$$0 \le \Delta\tau_{d,i}^{ch} \le My_{d,i}; \forall d \in 1 \dots N^d, \forall i \in \Omega_i \quad (28.c)$$

By linearizing (8) and (20), expression (11) is recast to (29).

$$\Delta t \sum_{d=1}^{N^d} \sum_{ki \in \Omega_{ur}} \sum_{t=1}^{N^P} \alpha_{d,ki,t} + \sum_{d=1}^{N^d} \sum_{i \in \Omega_i / t_{d,i}^n \ge 0} \Delta\tau_{d,i}^{ch} \le \tau^{max} + \Delta\tau \quad (29)$$

B. MILP Model

The MILP model of OSNMs of the HEV considering CO_2 emissions reduction levels is as follows:

$$min\ (4)$$

s.t.: (5)-(7),(9),(10),(12)-(16), (18), (19), (21)-(25),(26)-(29).

IV. Case Study and Results

To evaluate the proposed MILP model, the system presented in Fig. 1 is used. Also, $\overline{v}_{ki}$ is calculated by the algorithm shown in Fig. 3. The main features of the HEV can be found in [38]–[40] value of δ^D for the HEV is 0.8 (the difference between 0.9 and 0.1) times K^E divided by au. The initial state of charge of the HEV battery is equal to K^E, arriving at the warehouse with a value of δ^{PE} of 0.85. In addition, the HEV starts with K^C = 40 L and the fuel price is $3.65 per L [41]. To implement and solve the proposed model, AMPL [42] and the commercial solver CPLEX [43] are used, respectively. The total CPU time to find the global solution by the proposed algorithm using a 2.67-GHz computer with 3 GB of RAM is about 45.3 seconds. For each charging point, the value of P^{ch}, as well as $\underline{\tau}^{ch}$ and $\overline{\tau}^{ch}$, are considered to be 10 kW, and 0.3 h and 0.5 h, respectively [4], [25] The values of η^{rE} and η^{dE} are 0.98 and 1.00, [2], [24] For the MILP model, 5 emissions reduction levels, ρ^C, are used; the values of ρ^C for these levels are 10%, 20%, 30%, 40% and 50%, respectively. The coefficients related to maintenance costs, δ^{km}, and extra hour costs, δ^{hx}, presented in (4), are assumed to be set at within ratios 1 and 100, respectively, considering a greater weight for the extra hour coefficient. In the operation of the HEV, τ^{max} is 8 h (habitual working hours) [44]. In addition, Δt is 0.1 h, and the total number of periods, N^P, for each urban road *ki* to be traveled for delivery *d* is 10. All possible strategies to reach the delivery points, N^d, are available in [34]. For all possible strategies the HEV departs from and arrives at the warehouse, intersection 35. Thus, the matrix $MR_{r,d}$ for each possible strategy *r* and delivery *d* is obtained and used as input data of the flowchart shown below.

Fig. 4 shows the flowchart of the iterative process to evaluate the MILP model for each possible route *r* in each delivery *d*. This iterative process is run for each emissions level value, ρ^C, in the MILP model. To start the iterative process, the values of N^d, *NR*, and $MR_{r,d}$, and $t_{d,i}^n$ are initialized to zero. Applying the iterative process, the OSNMs of the HEV under the emissions reduction levels are obtained. Then, an iterative process is carried out for all possible routes, *r*, and the other iterative process related to delivery *d* is taken into account. For each

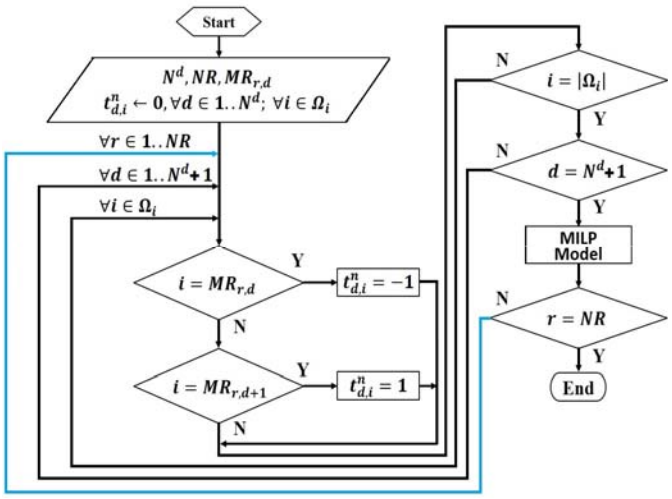

Fig. 4. Flowchart for the iterative process.

TABLE II
EXTRA HOURS VALUES GENERATED IN THE HEV OPERATION FOR DELIVERY 1

Route 1: 35 → 66 → 49 → 18 → 7 → 35					
ρ^C	10%	20%	30%	40%	50%
Extra hours (h)	2.27	2.90	3.52	4.14	4.76

TABLE III
SHORTEST ROUTE OF THE BEST STRATEGY FOR THE HEV

	Route 1 of the best strategy
Delivery 1	35 → 33 → 32 → 31 → 53 → 55 → 65 → 66
Delivery 2	66 → 56 → 52 → 51 → 50 → 49
Delivery 3	49 → 48 → 38 → 36 → 22 → 21 → 20 → 19 → 18
Delivery 4	18 → 1 → 2 → 3 → 4 → 5 → 6 → 7
Return	7 → 8 → 9 → 10 → 27 → 35

delivery d, an iterative process for all intersections i is also performed. The intersections are compared under the conditions $i = MR_{r,d}$, and $i = MR_{r,d+1}$. Depending on the value at intersection i, the conditions can be true or false, and values of -1 and 1 are assigned to $t^n_{d,i}$. Thereafter, each intersection i is compared under the condition $i = |\Omega_i|$. If the condition is *No*, then a new iteration for i is done, otherwise, each d is compared under a new condition $d = N^d + 1$; if this condition is *No*, then an iteration for the next d is performed. Otherwise, the MILP model is evaluated. Finally, r is compared under the condition $r = NR$ and if the condition is *No*, a new iteration for r is performed, otherwise, the process terminates.

After considering all possible routes, two representatives for the operating strategies, namely the best and the worst routes, are selected. The selection is due to the corresponding objective values, the values of the total navigated length and the extra hours, during the operation. Both routes are obtained for each emissions level, ρ^C. Figs. 5 (a)-(b) show the routes of the best (red) and worst (blue) operating strategies. In Fig. 5 (a) the best strategy is represented by route 1 (278 km), and deliveries are at intersections 66, 49, 18, 7, with a return to 35. The worst strategy is represented by route 15 (366 km) as shown in Fig. 5 (b). The charging points (gray squares) present at intersection i ($r^S_i = 1$) on each urban road ki to be traveled during navigation of the HEV are also shown for both strategies. The effect of different emission levels in extra hours is presented in Table II. It can be seen that, although increasing the emission levels increases the extra hours, the route remains the same. Table III

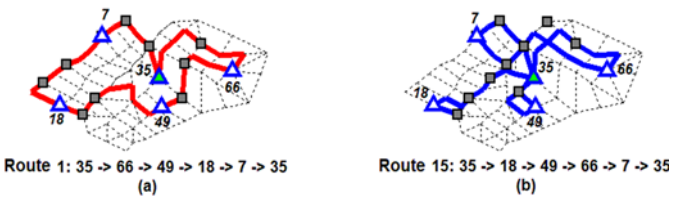

Fig. 5. Routes for the best and worst strategies.

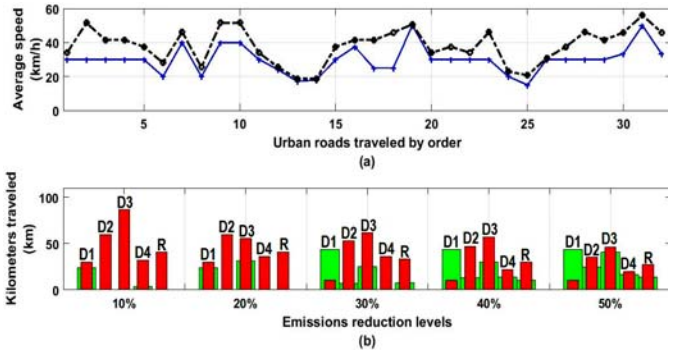

Fig. 6. Average speed and kilometers traveled by the HEV.

shows each urban road ki to be traveled for each delivery d and return to the warehouse. The direction of traffic, as well as the route chosen, have a strong influence on determining the shortest route of the HEV.

Figs. 6 (a)-(b) show the average speed and the total number of kilometers traveled for each emissions level, ρ^C. In Fig. 6 (a) blue and black-dashed lines represent $v_{d,ki}$ and $\overline{v}_{ki}$, respectively. These values of $v_{d,ki}$ are related to the best operating strategy that considers reaching the delivery points and return to the warehouse (represented in Fig. 6 (b) by letters D1, D2, D3, D4, and R, respectively). Moreover, urban roads with speed peaks (about 50 km/h) near $\overline{v}_{ki}$ indicate the presence of a lower traffic density during navigation of the HEV.

In Fig. 6 (b) red and green bars represent the values related to the kilometers traveled by the HEV in SM and DM, respectively. These bars are categorized into five groups and each group represents a ρ^C level. For each value of ρ^C, the kilometers traveled by the HEV are optimized so that at each emissions level the total number of kilometers traveled by the HEV in SM is reduced and, as a consequence, the optimal use of its battery is achieved for each delivery and return.

Figs. 7 (a)-(e) show the OSNMs of the HEV for the best operating strategy for each emissions reduction level. The black-dashed lines stand for the number of kilometers traveled by HEV in each urban road ki during navigation along the shortest route without considering the OSNMs, $d_{d,ki}\omega_{d,ki}$, (see Fig. 5 (a)). The red-dashed and green lines represent the number of kilometers traveled in SM ($d^{SM}_{d,ki}$) and DM ($d^{DM}_{d,ki}$), respectively, when the OSNMs are considered. Note that for each value of ρ^C, the MILP model determines the automation of the HEV navigation modes (SM and DM) during the operation strategy. The points in which the black-dashed and green lines have the same values represent the HEV navigation in DM (i.e. efficient use of battery), otherwise the HEV navigation is made considering the number of kilometers traveled in SM, and the remaining kilometers in DM, for each traveled urban road ki.

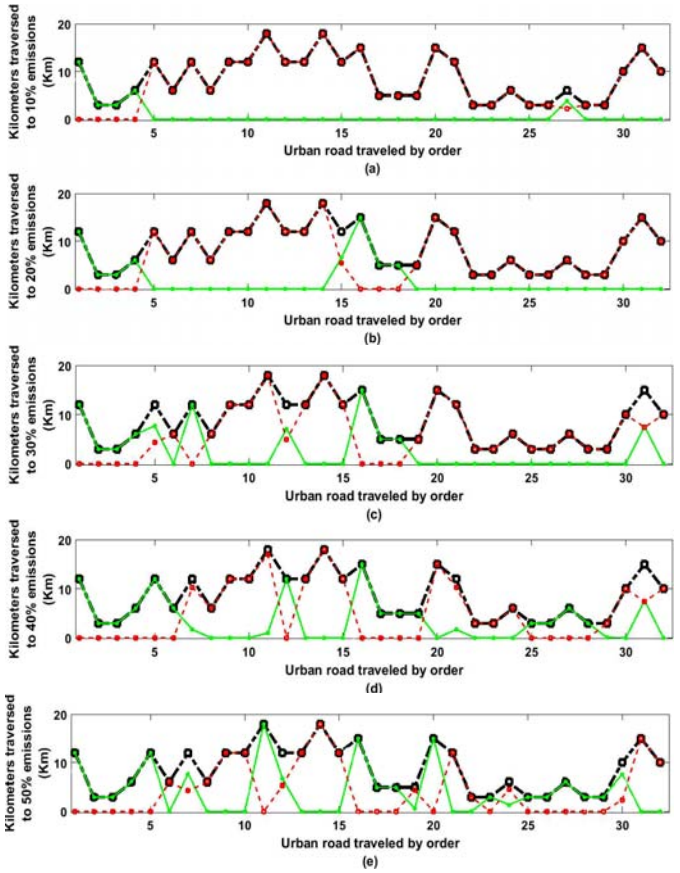

Fig. 7. Kilometers traveled by the HEV corresponding to each CO_2 emissions reduction level in SM and DM.

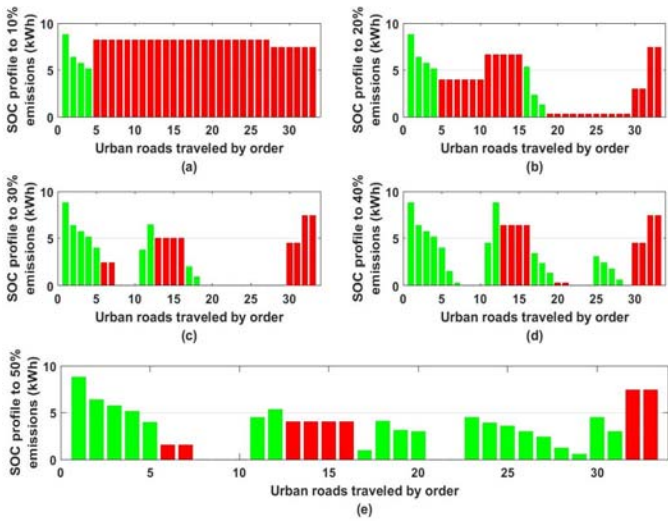

Fig. 8. Charge state profile of the HEV for each CO_2 emissions reduction level.

TABLE IV
CHARGING POINTS VISITED AND OPERATING TIMES OF THE HEV FOR CO_2 EMISSION REDUCTION LEVELS

ρ^C	Sequence of charging points visited	Total charging time (h)	Extra hours (h)	Total Oper. time (h)
10%	53	0.47	2.27	10.27
20%	51 → 9 → 27	1.10	2.90	10.90
30%	51→50→9→27	1.72	3.52	11.52
40%	51→50→4→9→27	2.34	4.14	12.14
50%	51→50→21→2→9→27	2.96	4.76	12.76

TABLE V
FUEL CONSUMPTION AND CORRESPONDING COSTS FOR EACH LEVEL OF CO_2 EMISSIONS REDUCTION

Fuel consumption (L)					
Without OSNMs	With OSNMs				
	10%	20%	30%	40%	50%
3.89	3.50	3.11	2.72	2.34	1.95
Fuel consumption costs ($)					
14.19	12.77	11.35	9.93	8.54	7.12

Figs. 8 (a)-(e) show the SOC profiles of the HEV for each ρ^C value. In these figures, green and red bars represent the SOC values when the HEV battery is efficiently used (DM) and when it is consuming fuel (SM), respectively. The SOC of the HEV in SM has two forms. In the first one, the HEV battery presents an SOC with a constant value for the set of bars in red, as shown in Fig. 8 (a), where, after battery usage (green bars), the SOC remains constant at 8 kWh (first set of red bars), and then this value is reduced to approximately 7.2 kWh (second set of red bars). The second form shows the HEV battery with SOC values near zero (Figs. 8 (b) and 8 (d)) or fully discharged, as shown in Figs. 8 (c)-(e). The efficient use of the HEV battery is more frequent as a consequence of the OSNMs during the shortest navigation route in the best operating strategy.

The sequence of charging points shown in Table IV indicates the order of the points visited during HEV navigation. Charging times, extra hours, and the total operating time for each CO_2 emissions reduction level as a result of the OSNMs of the HEV are also shown in Table IV. The difference between the total charging time and extra hours is 1.8 hours, which represents the total delay time due to the traffic density variation present on each urban road *ki* during operation of the HEV. This delay represents the sum of all time delays obtained in each urban road *ki* traveled during the HEV navigation. In addition, this delay time for each urban road *ki* is a consequence of the average speed variation, constraint (10), that presents a maximum limit calculated as a result of the algorithm proposed in Fig. 3. For most emissions levels, charging points 51 and 27 are frequently visited by the HEV. Hence, the location of charging point 27 which is nearest to the warehouse (see Fig. 1) ensures that the HEV battery has energy available (near to its energy storage capacity, K^E) for future operation strategies.

Table V shows fuel consumption and fuel consumption costs for the best operating strategy of the HEV with and without the OSNMs considering the level of CO_2 emissions reduction. The term "Without OSNMs" refers to the condition in which an HEV only navigates consuming fuel (i.e., SM mode). Moreover, fuel consumption values and their costs in HEV operation for both cases with and without OSNMs are related to the number of kilometers traveled, which are represented by red-dashed and black-dashed lines, respectively as shown in Figs. 7 (a)-(e). For an operating period of one day, HEV navigation without considering OSNMs generates a fuel consumption of 3.89 L. In the case of considering the OSNMs, the fuel consumption of the HEV is reduced by 0.39 L for each level of CO_2 emissions reduction. Thus, for a sustainable scenario a reduction in fuel consumption generates a significant savings of $7.07 for the highest emissions reduction during the best operating strategy of the HEV.

TABLE VI
DISTANCES TRAVELED BY THE HEV IN SM AND THE CORRESPONDING EMISSIONS FOR THE BEST OPERATING STRATEGY AT DIFFERENT LEVELS OF ρ^C

ρ^C (%)	Total kilometers (km)	Total emissions (gCO_2)
10	250.20	8006.4
20	222.40	7116.8
30	194.60	6227.2
40	166.80	5337.6
50	139.0	4448.0

Table VI presents the distances traveled by the HEV in SM and the corresponding emissions at different levels of ρ^C for the best operating strategy. These distances are far from 278 km, which is the best operating strategy obtained by the proposed model. From this table, the average amount of emissions is 6227.84 gCO_2, while if the HEV travels all the distance on fuel, the total emission is 8896.00 gCO_2. On the other hand, the average emissions level of a new traditional car sold in 2016 is 118.1 grams of CO_2 per kilometer (gCO_2/km) [45], [46]. Therefore, considering the same distance, the emissions are 32831.8 gCO_2. This value represents the total emissions of a new car sold in 2016 in Europe without a smart management system. It can be seen that 32831.8 gCO_2 compared to the average emissions obtained by our model under OSNMs, 6227.84 gCO_2, is a very high value. Therefore, this simple comparison shows the effectiveness of the proposed onboard management system.

V. CONCLUSIONS

This paper has proposed an MILP model to find the OSNMs (SM and DM) of an HEV as part of the operating strategy. The OSNMs are related to the operating strategy, which is composed of a reduction of CO_2 emissions levels, efficient battery recharges, and optimal scheduling of deliveries. The proposed model considers a set of operational and environmental constraints related to the scheduling of deliveries, average speed variation, battery capacity, charging and discharging rates, distances traveled in SM and DM, and CO_2 reduction levels. The probability values associated with the LOS are used to represent this variation during navigation of the HEV. A city map with 71 intersections and 131 urban roads, main and secondary, was used and, for each level of CO_2 emissions reduction, the OSNMs of the HEV were obtained at a minimum operational cost. The proposed model is useful for analyzing and improving the automation of HEV navigation systems, enabling companies to identify economic and sustainable alternatives in the implementation of hybrid transportation technology in various service areas, thereby ensuring less dependency on fossil fuels and encouraging the use of clean alternative sources.

Future work will consider applicable mechanisms to prevent unwanted congestion in roads.

REFERENCES

[1] L. Guo, B. Gao, Y. Gao, and H. Chen, "Optimal Energy Management for HEVs in Eco-Driving Applications Using Bi-Level MPC," *IEEE Trans. Intell. Transp. Syst.*, vol. 18, no. 8, pp. 2153–2162, Aug. 2017.

[2] C.-K. Chau, K. Elbassioni, and C.-M. Tseng, "Drive Mode Optimization and Path Planning for Plug-In Hybrid Electric Vehicles," *IEEE Trans. Intell. Transp. Syst.*, vol. 18, no. 12, pp. 3421–3432, Dec. 2017.

[3] Y. Gu, M. Liu, J. Naoum-Sawaya, E. Crisostomi, G. Russo, and R. Shorten, "Pedestrian-Aware Engine Management Strategies for Plug-In Hybrid Electric Vehicles," *IEEE Trans. Intell. Transp. Syst.*, vol. 19, no. 1, pp. 92–101, Jan. 2018.

[4] F. V. Cerna, M. Pourakbari-Kasmaei, R. A. Romero, and M. J. Rider, "Optimal Delivery Scheduling and Charging of EVs in the Navigation of a City Map," *IEEE Trans. Smart Grid*, vol. 9, no. 5, pp. 4815–4827, Sep. 2018.

[5] T. R. Board, Ed., *Highway Capacity Manual*. NW, Washington D. C.: National Academy of Sciences, 2010.

[6] X. Guo, J. Liu, and H. Fan, "Optimal charging navigation strategy for eElectric vehicles," in *2016 International Conference on Industrial Informatics - Computing Technology, Intelligent Technology, Industrial Information Integration (ICIICII)*, 2016, pp. 222–225.

[7] F. He, D. Wu, Y. Yin, and Y. Guan, "Optimal Deployment of Public Charging Stations for Plug-in Hybrid Electric Vehicles," *Transp. Res. Part B Methodol.*, vol. 47, pp. 87–101, Jan. 2013.

[8] W. Wei, L. Wu, J. Wang, and S. Mei, "Network Equilibrium of Coupled Transportation and Power Distribution Systems," *IEEE Trans. Smart Grid*, vol. 9, no. 6, pp. 6764–6779, Nov. 2018.

[9] C. Kurtulus and G. Inalhan, "Model Based Route Guidance for Hybrid and Electric Vehicles," in *2015 IEEE 18th International Conference on Intelligent Transportation Systems*, 2015, pp. 1723–1728.

[10] S. Ebbesen, M. Salazar, P. Elbert, C. Bussi, and C. H. Onder, "Time-Optimal Control Strategies for a Hybrid Electric Race Car," *IEEE Trans. Control Syst. Technol.*, vol. 26, no. 1, pp. 233–247, Jan. 2018.

[11] M. F. M. Sabri, K. A. Danapalasingam, M. F. Rahmat, and M. Ridzuan Md Yusof, "Fuel economy analysis of a through-the-road hybrid electric vehicle," in *2015 10th Asian Control Conference (ASCC)*, 2015, pp. 1–6.

[12] E. Yudovina and G. Michailidis, "Socially Optimal Charging Strategies for Electric Vehicles," *IEEE Trans. Automat. Contr.*, vol. 60, no. 3, pp. 837–842, Mar. 2015.

[13] C. Rottondi, G. Neglia, and G. Verticale, "Complexity Analysis of Optimal Recharge Scheduling for Electric Vehicles," *IEEE Trans. Veh. Technol.*, vol. 65, no. 6, pp. 4106–4117, Jun. 2016.

[14] Y. Tang, J. Zhong, and M. Bollen, "Aggregated Optimal Charging and Vehicle-to-grid Control for Electric Vehicles Under Large Electric Vehicle Population," *IET Gener. Transm. Distrib.*, vol. 10, no. 8, pp. 2012–2018, May 2016.

[15] A.-D. Ourabah, B. Quost, A. Gayed, and T. Denoux, "Estimating energy consumption of a PHEV using vehicle and on-board navigation data," in *2015 IEEE Intelligent Vehicles Symposium (IV)*, 2015, pp. 755–760.

[16] S. Mehar, S. Zeadally, G. Remy, and S. M. Senouci, "Sustainable Transportation Management System for a Fleet of Electric Vehicles," *IEEE Trans. Intell. Transp. Syst.*, vol. 16, no. 3, pp. 1401–1414, Jun. 2015.

[17] J. Liu and Y. Chen, "An online energy management strategy of parallel plug-in hybrid electric buses based on a hybrid vehicle-road model," in *2016 IEEE 19th International Conference on Intelligent Transportation Systems (ITSC)*, 2016, pp. 927–932.

[18] J. Yang and G. Zhu, "Stochastic Predictive Boundary Management for a Hybrid Powertrain," *IEEE Trans. Veh. Technol.*, vol. 65, no. 6, pp. 4700–4713, Jun. 2016.

[19] C. M. Martinez, X. Hu, D. Cao, E. Velenis, B. Gao, and M. Wellers, "Energy Management in Plug-in Hybrid Electric Vehicles: Recent Progress and a Connected Vehicles Perspective," *IEEE Trans. Veh. Technol.*, vol. 66, no. 6, pp. 4534–4549, Jun. 2017.

[20] L. Li, C. Yang, Y. Zhang, L. Zhang, and J. Song, "Correctional DP-Based Energy Management Strategy of Plug-In Hybrid Electric Bus for City-Bus Route," *IEEE Trans. Veh. Technol.*, vol. 64, no. 7, pp. 2792–2803, Jul. 2015.

[21] J. Lohrer, M. Forth, and M. Lienkamp, "A data-driven predictive energy management strategy for plug-in hybrid vehicles," in *2017 International Conference on Mechanical, System and Control Engineering (ICMSC)*, 2017, pp. 297–304.

[22] X. Zeng and J. Wang, "Stochastic optimal control for hybrid electric vehicles running on fixed routes," in *2015 American Control Conference (ACC)*, 2015, pp. 3273–3278.

[23] W. Zhou, C. Zhang, J. Li, and H. K. Fathy, "A Pseudospectral Strategy for Optimal Power Management in Series Hybrid Electric Powertrains," *IEEE Trans. Veh. Technol.*, vol. 65, no. 6, pp. 4813–4825, Jun. 2016.

[24] Z. Darabi, P. Fajri, and M. Ferdowsi, "Intelligent Charge Rate

Optimization of PHEVs Incorporating Driver Satisfaction and Grid Constraints," *IEEE Trans. Intell. Transp. Syst.*, vol. 18, no. 5, pp. 1325–1332, May 2017.

[25] C. Li, Q. Liu, L. Guo, and H. Chen, "Fuel economy optimization of hybrid electric vehicles," in *The 27th Chinese Control and Decision Conference (2015 CCDC)*, 2015, pp. 810–815.

[26] H. S. Kasana and K. D. Kumar, *Introductory Operations Research*. Berlin, Heidelberg: Springer Berlin Heidelberg, 2004.

[27] "Summary of State Speed Laws," 2012. [Online]. Available: https://www.nhtsa.gov/sites/nhtsa.dot.gov/files/documents/summary_state_speed_laws_12th_edition_811769.pdf.

[28] "Brazilian Traffic Code (CTB)," 2015. [Online]. Available: http://portaldotransito.com.br/noticias/voce-sabe-como-e-determinada-a-velocidade-maxima-das-rodovias/.

[29] "The Road to Sustainable Urban Logistics," 2017. [Online]. Available: https://sustainability.ups.com/media/UPS_The_Road_to_Sustainable_Urban_Logistics.pdf.

[30] "Logistics Optimization: Warehouse Desing and Layout," 2018. [Online]. Available: https://www.ups.com/us/en/services/customized-solutions/optimization-logistics/warehouse-design.page?

[31] K. Morrow, D. Karner, and J. Francfort, "Plug-in Hybrid Electric Vehicle Charging Infrastructure Review," 2009. [Online]. Available: https://trid.trb.org/view.aspx?id=894452.

[32] M. Spöttle *et al.*, "Research for TRAN Committee- Charging infrastructure for electric road vehicles," 2018. [Online]. Available: http://www.europarl.europa.eu/RegData/etudes/STUD/2018/617470/IPOL_STU(2018)617470_EN.pdf.

[33] B. Andrasfai, *Graph Theory: Flows, Matrices*, First ed. CRC Press, 1991.

[34] "Data." [Online]. Available: https://drive.google.com/file/d/0B1nRtHmm8AupVWtOd2p3RW5LTEk/view?usp=sharing.

[35] L. Elefteriadou, *An Introduction to Traffic Flow Theory*, vol. 84. New York, NY: Springer New York, 2014.

[36] "Brazilian Traffic Code (CTB)," 2015. .

[37] P. S. Iyer, *Operational Research*. McGraw Hill Education, 2008.

[38] "Prius Prime Toyota– Features," 2018. [Online]. Available: https://www.toyota.com/priusprime/ebrochure.

[39] "Tesla Motors– Model Specifications," 2018. [Online]. Available: http://www.teslamotors.com/models/specs.

[40] "IA-HEV: Hybrid and Electric Vehicle Technologies," 2018. [Online]. Available: http://www.ieahev.org/.

[41] "Brazil– Global Petrol Prices." [Online]. Available: http://pt.globalpetrolprices.com/Brazil/gasoline_prices/.

[42] R. Fourer, D. M. Gay, and B. W. Kernighan, "AMPL: A Modeling Language for Mathematical Programming," Nov-2018. [Online]. Available: https://ampl.com/.

[43] "IBM ILOG CPLEX Optimization Studio," 2018. [Online]. Available: https://www.ibm.com/fi-en/marketplace/ibm-ilog-cplex.

[44] "U.S. Department of Labor – Wage and Hour Division (WHD)." [Online]. Available: https://www.dol.gov/whd/state/meal.htm.

[45] "Road Transport: Reducing CO2 Emissions from Vehicles." [Online]. Available: https://ec.europa.eu/clima/policies/transport/vehicles/cars_en.

[46] "CO_2 Emissions from Fuel Combustion 2017 – Highlights - IEA." [Online]. Available: https://www.iea.org/publications/freepublications/publication/CO2EmissionsfromFuelCombustionHighlights2017.pdf.